RSC Advances

PAPER

Check for updates

Self-assembly of amphiphilic poly(styrene-*b*-acrylic acid) on magnetic latex particles and their application as a reusable scale inhibitor†

Chariya Kaewsaneha, [ID] *[a] Abdelhamid Elaissari,[b] Pramuan Tangboriboonrat[c] and Pakorn Opaprakasit [ID] *[a]

The deposition of scale on membranes or container and pipe surfaces (clogging the system) is a costly issue in water treatment processes or water-cooling systems. To effectively cope with this issue, magnetic polymeric nanoparticles (MPNPs) have been developed and applied as promising scale inhibitors, due to their high surface-area-to-volume ratio, surface modifiability, and magnetic separation ability. Carboxylated MPNPs, having a monodisperse size distribution (236 ± 26 nm) with a high magnetic content of 70 wt% and superparamagnetic properties, were fabricated by using a 2-step process: (i) formation of clusters of hydrophobic magnetic nanoparticles stabilized by oleic acid (OA-MNPs), and (ii) self-assembly of the amphiphilic block copolymer of poly(styrene$_{27}$-*b*-acrylic acid$_{120}$) (PS$_{27}$-*b*-PAA$_{120}$) onto the cluster surfaces. With application of ultrasonication to 12.0 wt% OA-MNPs, a three-dimensional network was formed by particle–particle interactions, suppressing coalescence, and then creating stable magnetic clusters. The cluster surfaces were then adsorbed by amphiphilic PS$_{27}$-*b*-PAA$_{120}$ *via* the attractive force between hydrophobic PS blocks. This moves longer hydrophilic PAA blocks containing carboxylic acid groups into the water phase. The formulated MPNPs acted as a nanosorbent for calcium ion (Ca^{2+}) removal with a removal efficiency of 92%. The MPNPs can be effectively reused for up to 4 cycles. Based on the electrostatic interactions between the negatively-charged polymer and the hydrated Ca^{2+}, the resulting precipitation leads to the prevention of calcium carbonate scale formation. Insights into this mechanism open up a new perspective for magnetic-material applications as effective antiscalants.

1. Introduction

Mineral deposits, formed by ionic reactions, result in the formation of an insoluble precipitate. For example, when hard water is heated, calcium ions (Ca^{2+}) react with bicarbonate (HCO$_3^-$) ions to form insoluble calcium carbonate (CaCO$_3$). This precipitate, known as scale, can cause serious problems in infrastructures, such as hot-water pipes, heaters, boilers, and cooling systems. As scale builds up, water flow is impeded; hence, appliance parts and pipes must be cleaned or replaced.[1–3] Development of water treatment processes by removal of Ca^{2+} before use is of interest, to prevent the deposition of inorganic scaling and particulate fouling in the system.

Generally, hydrophilic polymers, *e.g.*, poly(acrylic acid) (AA), poly(acrylic acid-*co*-maleic acid), acrylic acid-*co*-2-acrylamido-2-methyl-propane sulfonate (AA-*co*-AMPS) copolymer, and green scale inhibitors, *e.g.*, poly(aspartic acid) and poly(epoxysuccinic acid) are widely used for this purpose.[4–6] These compounds contain abundant active functional groups, such as carboxyl and amino groups, and exhibit good scale-inhibition performance due to their efficient chelation, dispersion, and lattice distortion.[7] Inhibitor molecules can stabilize complexes or particles in an aqueous solution in a surfactant-like fashion. The mechanisms of nucleation and crystal growth control are based on: (i) prevention of nucleation through ion complexation, (ii) prevention of nucleation by stabilization of pre-nucleation clusters, and (iii) surface stabilization of precursor particles in the nanometer regime by surface coordination.[5–8] For example, the sulfonated side chain of AMPS is a superior solubilizing group over the whole pH range. This can stabilize aggregates or particles in solution, while the carboxylate groups interact with solvated or surface-bound Ca^{2+} ions. Thus, AA-*co*-AMPS copolymers can be used to control scale formation even under high ionic strength conditions.[5] Liu *et al.* reported a novel process for synthesis of maleic anhydride-allylpolyethoxy

a School of Bio-Chemical Engineering and Technology, Sirindhorn International Institute of Technology (SIIT), Thammasat University, Pathum Thani 12121, Thailand. E-mail: chariya@siit.tu.ac.th; pakorn@siit.tu.ac.th

b Univ Lyon, University Claude Bernard Lyon-1, CNRS, LAGEPP-UMR 5007, F-69622 Lyon, France

c Department of Chemistry, Faculty of Science, Mahidol University, Rama 6 Road, Phyathai, Bangkok 10400, Thailand

† Electronic supplementary information (ESI) available. See DOI: 10.1039/d0ra06334g

carboxylate copolymer for inhibition of $CaCO_3$ formation in industrial cooling systems.[9] Owing to their hydrophilic nature and high capacity in dispersing in water, the carboxyl groups in the copolymer chains could recognize and encapsulate or react with positively-charged Ca^{2+} ions either in solutions or on the surface of inorganic $CaCO_3$ crystals. As a consequence, the aggregation of $CaCO_3$ solid particles was blocked. The copolymers showed high antiscalant efficiency of 98%, even at a low application dosage of 8 mg L^{-1}. However, after complexing with cations, these copolymers cannot be separated or reused, but are discharged to the water resources, which may cause serious problems to the environment.

Adsorption, which is a simple and convenient process providing high removal efficiency, is preferable for the elimination of heavy metal ions. Utilization of magnetic nanomaterials (MNMs) as nanosorbents has received much attention, due to their magnetic separation properties, small size, high surface-area-to-volume ratio, and surface modifiability.[10] The separation of metal ions adsorbed on MNMs from treated aqueous solutions under external magnetic field (without any sludge formation), is advantageous. The adsorption efficiency depends on types of functional groups, polarity, surface area, and porosity of the nanosorbents. Do *et al.* reported a synthesis of MNMs by encapsulation of iron oxide nanoparticles in maleic acid-2-acrylamido-2-methyl-1-propanesulfonate copolymer *via* an inverse miniemulsion polymerization, for use in oilfield scale-inhibition applications.[11] With a concentration of 5 ppm, MNMs could inhibit carbonate scale deposition up to 63.6%. The authors demonstrated that the inhibition activity of MNMs was higher than that of the parent copolymer and could be easily detected in produced water by magnetic monitoring devices after being used in oilfields. However, the reusability of MNMs has not been investigated. Moreover, when the materials were prepared by stabilizing single iron oxide nanoparticle with the copolymer, their small-sized magnetic domain caused slow magnetic separation and a time-consuming process. A promising technique to overcome this issue is based on the design of MNMs with high iron oxide nanoparticles encapsulated into polymer particles (functionalized by active groups).[12,13]

Magnetic nanosorbents or magnetic polymeric nanoparticles (MPNPs) have been prepared by a wide range of techniques, including miniemulsion and seed emulsion polymerizations.[14–17] In our previous work, MPNPs self-functionalized with carboxylic groups were fabricated *via* a miniemulsion polymerization.[14,15] Briefly, iron oxide (Fe_3O_4) or magnetic nanoparticles (MNPs) were coated with oleic acid (OA), designated as OA-MNPs. The OA-MNPs were mixed with styrene (St), divinylbenzene (DVB), and acrylic acid (AA) monomers before emulsification using potassium persulfate as the initiator. The resulting MPNPs (~200 nm) were functionalized with carboxylic groups from AA, showing a uniform distribution of iron oxide (53 wt%) in the polymer matrix. Alternatively, the formation of magnetic clusters prior to their encapsulation is an effective strategy to obtain hybrid particles with a high magnetic content, endowing them with a fast magnetic response. To generate MPNPs with a high magnetic content, seed emulsion

polymerization using a magnetic emulsion (an organic ferro-fluid of OA-MNPs emulsified in an aqueous medium by Triton X-405) as a seed was introduced.[16,17] The content of magnetic material inside the polymer particles can be controlled at the beginning of magnetic seed emulsion formation. In the process, St and DVB monomers containing 2,2′-azobis(2-isobutyronitrile) initiator were diffused inside the magnetic seed emulsion before being polymerized. Hybrid MPNPs with a high magnetic content (>60 wt%) were produced. However, such techniques require multiple washing steps to isolate the purified products from the reaction media and unreacted monomers. Loss of super-paramagnetization is observed, likely due to the oxidizing and thermally-aggressive initiation/polymerization conditions. Moreover, the complicated *in situ* chemical or polymerization techniques are time-consuming.

An alternative approach to encapsulate MNPs in a polymer matrix involves spontaneous self-assembly of the magnetic core and amphiphilic block copolymer (ACP) shell nano-structures.[18–21] The facile self-assembly technique is offered as a powerful route to the formation of the hybrid MPNPs. The hybrid particle formation is postulated to utilize a nucleation-aggregation mechanism after a solvent switch from a good solvent to a non-solvent. Kim *et al.* demonstrated that amphiphilic poly(styrene$_{250}$-b-acrylic acid$_{13}$) (PS_{250}-b-PAA$_{13}$) can be assembled around a cluster of hydrophobic MNPs to enclose the particle within copolymer micelles by a co-precipitation method. The assembly of MNPs and ACP was achieved in a selective solvent.[19] PS_{250}-b-PAA$_{13}$ was first dissolved in N,N-dimethylformamide, a good solvent for both the hydrophobic PS and hydrophilic PAA blocks, and combined with a solution of MNPs in tetrahydrofuran at a desired ratio. Water, a selective non-solvent for both the hydrophobic MNPs and PS blocks, was then gradually added to this mixture to desolvate both species, leading to the formation of micelle-like structures or clusters around the MNPs. The presence of hydrophilic PAA blocks could stabilize the hybrid particles. The number of MNPs per cluster was controlled by varying the initial relative concentration of MNPs and the polymers. However, the maximum number of MNPs per cluster was *ca.* 23 particles. The PAA shell, however, required further chemical crosslinking to stabilize the particle structure and protect the loss of MNPs. In fact, the use of ACPs with longer hydrophilic segments leads to a formation of stable hybrid MPNPs, due to thick hydrophilic shell.[20]

In this work, MPNPs consisting of carboxylic acids, which possess a high magnetic content and well-defined morphology, are formulated by using a facile self-assembly process. A hydrophobic OA-MNP emulsion, with St acting as an oil phase, is first prepared by employing an ultrasonication-assisted process. By adding an ACP solution containing long hydrophilic blocks of PS_{27}-b-PAA$_{120}$ into the emulsion, the ACP can self-assemble to adsorb onto and stabilize the cluster surfaces, resulting in the formation of carboxylated MPNPs. The effects of the contents of OA-MNPs and the copolymer on properties of the resulting MPNPs, *i.e.*, stability, chemical compositions, magnetic contents, and magnetic properties, are investigated. The synthesized carboxylated MPNPs are employed as anti-scalants for the removal of Ca^{2+} from hard water that contains

calcium and carbonate ions. The Ca^{2+} removal efficiency and reusability of the synthesized MPNPs are examined.

2. Experimental

2.1 Materials

Styrene (St) monomer (Sigma-Aldrich, Purum), iron(III) chloride ($FeCl_3$) (Riedel-deHaën), iron(II) chloride tetrahydrate ($FeCl_2 \cdot 4H_2O$) (Sigma Aldrich, Purum), 25% ammonium hydroxide solution (NH_4OH) (Merck, AR), oleic acid (OA) (Fluka, natural, from suet), calcium chloride ($CaCl_2$) (Ajax, AR), sodium bicarbonate ($NaHCO_3$) (Carlo Erba, analysis), and citric acid (Carlo Erba, analysis) were used as received. Poly(styrene$_{27}$-b-acrylic acid$_{120}$) (PS$_{27}$-b-PAA$_{120}$) was prepared according to the reported procedure.[22] Commercial carboxyl-based antiscalants, i.e., 2-phosphonobutane 1,2,4-tricarboxylic acid (PBTC) and maleic homopolymer (PMA) were supplied by Water Doctor (Bangkok, Thailand), and low molecular weight polyacrylic acid (Acumer 1050) was supplied by Rohm and Haas Chemicals (Thailand). Deionized (DI) water was used throughout this work.

2.2 Preparation of magnetic polymeric particles

Magnetic nanoparticles, coated with oleic acid (OA-MNPs) with an average diameter of 20 nm, were prepared via the co-precipitation of $FeCl_3/FeCl_2 \cdot 4H_2O$ (molar ratio of 2 : 1) with NH_4OH. The precipitated MNPs were then mixed with OA and stirred for 10 min, as described elsewhere.[14,15] After washing with ethanol for removing excess OA, the OA-MNPs at different concentrations, i.e., 2.5, 5.0, 7.5, and 12.0 w/v% were dispersed in St monomer (1 mL). These OA-MNPs were emulsified in DI water (pH 10; 10 mL) by ultrasonication at 70 (amplitude) for 10 min. In parallel, an aqueous solution of amphiphilic PS$_{27}$-b-PAA$_{120}$ at various concentrations, i.e., 0.1, 0.5, and 1.0 wt% was prepared at pH 10. The polymer solution (5 mL) was then immediately dropped into the magnetic emulsion, under homogeneous stirring. After homogenization for 1 h, the emulsion of magnetic clusters (stabilized by PS$_{27}$-b-PAA$_{120}$ or magnetic polymeric particles (MPNPs)) was slowly evaporated to remove residue St monomer under a fume hood for overnight. The resulting MPNPs were then purified by magnetic washing before characterizations.

2.3 Characterizations

The particle size, size distribution, and zeta potential of the MPNPs were determined by a microelectrophoresis apparatus (Zetasizer; Malvern, Nano ZS). The particle morphology was studied by using a transmission electron microscope (TEM; FEI, TECNAI G2), operated at an accelerating voltage of 120 kV. The chemical compositions of the materials were analyzed by Fourier transform infrared spectrometry in an attenuated total reflection mode (ATR-FTIR; Perkin Elmer, FrontierTM). The magnetic content was determined by thermogravimetric analysis (TGA, NETZSCH TG 209F1). The saturation magnetization (M_s) of the resulting particles was obtained from their magnetization curve, measured by a vibrating sample magnetometer (VSM, Lake Shore, 7403), under a magnetic field of up to 10 kOe, at room temperature.

2.4 Adsorption and desorption efficiency

The Ca^{2+} adsorption efficiency of the prepared MPNPs was evaluated based on the China National Standard method (GB/T 16632-2008). The prepared MPNPs (80 ppm dosage) were added into an aqueous solution of $CaCl_2$ mixed with $NaHCO_3$, with Ca^{2+} and HCO_3^- concentrations of 250 ppm. After adjusting the pH to 9.0 by using a borate buffer solution, the mixture was kept at 80 °C in a water bath, whose temperature was monitored by an electronic contact thermometer probe for 10 h.[9,23] The measurement was conducted at pH 9.0, which is in a typical range (8.0–10.0) used in industrial cooling systems. The MPNPs, adsorbed with Ca^{2+}, were then separated from the medium by applying an external magnetic field. The adsorbed MPNPs were transferred into a 100 mL conical flask containing a 0.1 M citric acid solution (25 mL), and shaken (IKA, VIBRAX VXR basic) at room temperature for 1 h. A similar magnetic separation was applied to collect MPNPs after each washing step by using DI water. The materials were then reused in subsequent adsorption experiments. The concentration of the remaining Ca^{2+} in the solution was measured using inductively coupled plasma (ICP) spectrometry (PerkinElmer Optima 8000, emission mode).

2.5 Scale-inhibition performance of MPNPs

$CaCO_3$ scale-inhibition performance of the MPNPs (80 ppm dosage) was examined under the same conditions of the adsorption and desorption efficiency tests. After incubation and separation of the adsorbed MPNPs, the solution was filtered to remove precipitates. The concentration of Ca^{2+} ions from the desorbed MPNPs and that in the solution was determined by an ICP technique. The performance of commercial carboxyl-based antiscalants, at a practical dosage of 20 ppm, i.e., 2-phosphonobutane 1,2,4-tricarboxylic acid (PBTC), maleic homopolymer (PMA), and low molecular weight polyacrylic acid (Acumer 1050), and a blank test (without addition of antiscalants) were also measured using the same procedures. The scale-inhibition efficiency was calculated by following equation:[9,23]

$$\text{Inhibition efficiency (\%)} = \frac{[Ca^{2+}]_{final} - [Ca^{2+}]_{blank}}{[Ca^{2+}]_{initial} - [Ca^{2+}]_{blank}} \times 100$$

where $[Ca^{2+}]_{final}$ is the concentration of Ca^{2+} ions in the filtrate and desorbed MPNPs from the system with MPNPs antiscalant, $[Ca^{2+}]_{initial}$ is the concentration of Ca^{2+} ions at the beginning of the experiment, and, $[Ca^{2+}]_{blank}$ is the concentration of Ca^{2+} ions in the filtrate in the system without antiscalants.

The inhibition tests for each sample were repeated for 3 times, whose average value was reported. The morphology and elemental compositions of the precipitated $CaCO_3$ scales were investigated under scanning electron microscopy (SEM) and energy-dispersive X-ray spectroscopy (EDX).

3. Results and discussion

3.1 Fabrication of MPNPs

3.1.1 Effect of OA-MNPs contents. Morphology of the MPNPs, prepared by using different OA-MNP contents, were examined. TEM images of MPNPs, prepared at 2.5, 5.0, 7.5, and

12.0 w/v% OA-MNPs contents with a fixed PS_{27}-b-PAA_{120} composition of 1.0 wt%, are shown in Fig. 1(A–D).

At a low OA-MNPs content of 2.5 w/v%, MPNPs and particles of neat PS_{27}-b-PAA_{120} without OA-MNPs were separately formed (Fig. 1A). When the OA-MNPs contents were increased (5.0 and 7.5 w/v%) (Fig. 1B and C), OA-MNP aggregates were observed with irregular shapes. A further increase in the OA-MNPs content (12.0 w/v%), however, leads to the formation of uniform (spherical) particles (Fig. 1D). As schematically shown in Fig. 2, the formation of hybrid MPNPs consists of 2 steps: (i) formation of stable clusters of OA-MNPs or a magnetic emulsion as a result of ultrasonic-assisted emulsification, and (ii) self-assembly of amphiphilic PS_{27}-b-PAA_{120} molecules onto the cluster surfaces by changing its solubility.

Due to the hydrophobic nature of OA-MNPs, nano-precipitation of these particles in an aqueous phase (oil-in-water or o/w emulsion) can be achieved when the medium is switched from a good solvent (St monomer) to its non-solvent counterpart (water). This presumably minimizes their energetically unfavorable solvophobic interactions. Although this o/w emulsion system is thermodynamically unfavorable, the application of high-energy mixing from ultrasonication can overcome the local energy. The only feasible choice for the nanoparticles to locate is on the oil droplets, rather than in the water phase, by adsorbing to the oil–water interface and forming a dense film (monolayer or multilayer) on the droplets.[24–26] At high amounts of OA-MNPs (12.0 w/v%), a three-dimensional network is formed by particle–particle interactions, suppressing coalescence and generating a stable emulsion without the use of organic surfactants. This explanation is supported by dynamic light scattering (DLS) results, which reflect that the prepared clusters have an average size of 165 nm with monodispersity (Fig. S1†). Similarly, it was reported that hydrophobic SiO_2 nanoparticles with an average diameter of 20 nm could precipitate and effectively stabilize an o/w emulsion or clusters of hydrophobic SiO_2 nanoparticles in an aqueous phase. The reported procedure used ultrasonication with appropriate SiO_2 nanoparticles (3 wt% based on St monomer) and a volume ratio of St : water of 1 : 10.[27] It is noted that the presence of Fe_3O_4 magnetic nanoparticles under ultrasonication may lead to the conversion of St monomers to polystyrene (PS), due to redox polymerization. G. Qiu $et\ al.$ reported that 67% of St monomers were converted in 15 min in the presence of 0.3 g Fe_3O_4 nanoparticles.[28] This was due to the dissociation of Fe_3O_4 nanoparticles, producing Fe^{2+} ions. At the same time, the sonolysis of water generated H_2O_2, which subsequently reacted with Fe^{2+} to produce hydroxyl radicals and initiate the polymerization.

When amphiphilic PS_{27}-b-PAA_{120} (1.0 wt%) was dissolved in water at pH 10, the turbidity of the solution was increased.
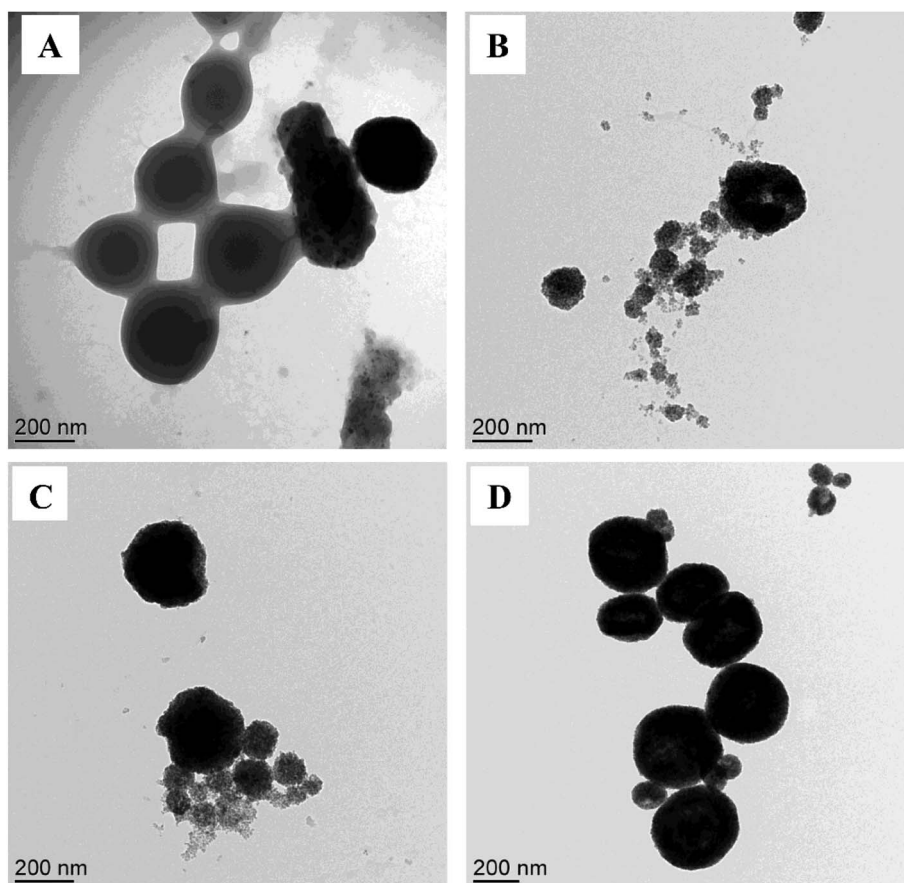

Fig. 1 TEM images of MPNPs, prepared from different OA-MNPs contents: (A) 2.5, (B) 5.0, (C) 7.5, and (D) 12.0 w/v%, with a fixed PS_{27}-b-PAA_{120} content of 1.0 wt%.
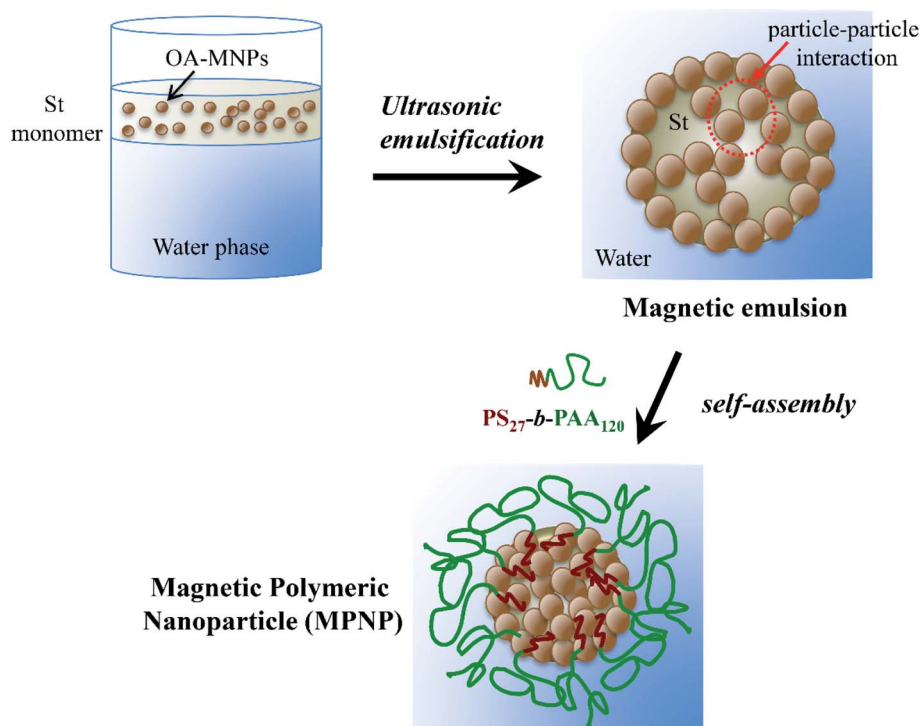
Fig. 2 Schematic representation of MPNP formation.

Given the results from an amphiphilic small-molecule system, micelles should be formed with a small dense core and a very large shell.[29] However, the polymer micelles generated in this state could not be examined by the DLS measurement. The amphiphilic PS_{27}-b-PAA_{120} may not form micellular structures in a basic solution. This asymmetric copolymer with longer hydrophilic (PAA) blocks is swollen by water molecules (a good solvent), preventing the aggregation of hydrophobic PS blocks due to steric effects. As pointed out by Rannard *et al.*, when the hydrophobic–hydrophilic balance (HLB) was interrupted in favor of the hydrophilic block segments of poly(ethylene glycol-b-2-hydroxypropyl methacrylate) (PEG_{113}-b-$HPMA_{50}$), a solution with poor light scattering was formed. This implies that limited self-assembly of the collapsed hydrophobic polymer segments occurs during the solvent polarity switch.[30]

When a polymer solution was added into a stable magnetic emulsion (12.0 w/v%) in which St and/or PS was retained on the droplets, the hydrophobic PS blocks adsorb onto the magnetic emulsion surface by the hydrophobic attractive force. Moreover, the St-rich phase may induce the PS blocks to strongly adsorb on the emulsion. The solvent (St) was polymerized, generating PS blocks which may be strongly fixed into the magnetic clusters. At the same time, the interaction between the hydrophilic PAA blocks and water molecules may be responsible for the stabilization of the particles. Due to longer hydrophilic PAA blocks, the thick hydrophilic shell stabilizes the hybrid particles in the aqueous phase and effectively prevents the loss of nanoparticles without chemical crosslinking.[20] This hypothesis is confirmed by their well-defined spherical morphology under TEM (Fig. 1D) when the separation and re-dispersion steps

employing an external magnetic field for several times were employed.

In contrast, when the polymer solution was added into unstable magnetic emulsions (low OA-MNPs content, 2.5 w/v%), the particle–particle interactions decreased. The long-distance van der Waals attractions between the nanoparticles are not strong enough to suppress the coalescence. Therefore, the St monomer and/or PS could not be retained in the droplets.[25–27] The swollen amphiphilic PS_{27}-b-PAA_{120} may adsorb St monomer and/or PS due to its high solubility, leading to the formation of new polymeric particles (Fig. 1A). The hydrophobic OA-MNPs were not allowed to participate in the polymer particle formation due to their incompatibility, resulting in aggregation or fragmenting of OA-MNPs in the system.

3.1.2 Effects of PS_{27}-b-PAA_{120} contents. To study the effects of the amphiphilic PS_{27}-b-PAA_{120} contents on the morphology of the hybrid particles, PS_{27}-b-PAA_{120} was dispersed in DI water (pH 10) at various concentrations. Hybrid MPNPs were prepared by using PS_{27}-b-PAA_{120} at concentrations of 0.1, 0.5, and 1.0 wt%, at a fixed OA-MNP content of 12.0 w/v%. Their morphologies were observed under TEM, as shown in Fig. 3(A)–(C). The TEM images show that an increase in the concentration of PS_{27}-b-PAA_{120} tends to generate uniform and spherical particles. At a low concentration of 0.1 wt%, the adsorbed PS_{27}-b-PAA_{120} could not completely cover the magnetic emulsion's surface and overcome the mechanical stirring shear force, resulting in broken and coalescent particles. When the PS_{27}-b-PAA_{120} content was increased to 0.5 wt%, spherical particles, with a broad size distribution, were produced. Moreover, a closer examination of small particles found that OA-MNPs
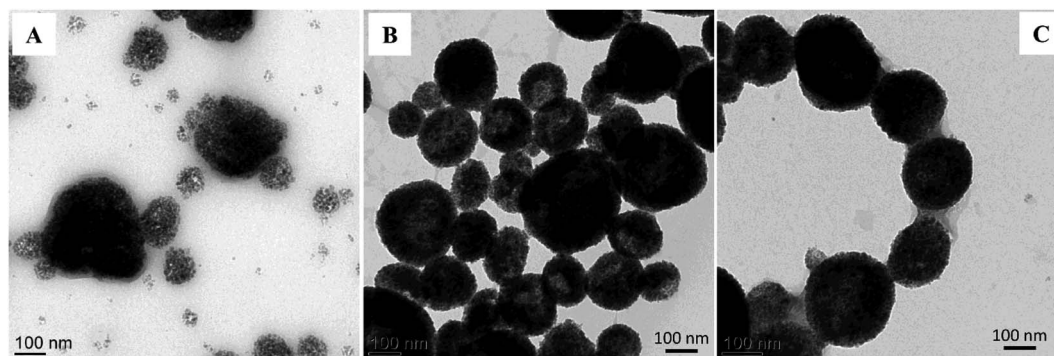
Fig. 3 TEM images of the prepared hybrid MPNPs, using PS$_{27}$-b-PAA$_{120}$ at different concentrations: (A) 0.1, (B) 0.5, and (C) 1.0 wt%, at a fixed OA-MNPs content of 12.0 w/v%.

(dark phase) were loosely packed inside the particles, compared to that of the larger-sized counterparts. This is in good agreement with the assumption that the primary magnetic emulsion may break, and a regenerate irregular hybrid particles.

The formation of hybrid particles can be described in terms of energetic contributions by the Gibbs free energy equation, as presented in eqn (1).[20]

$$\Delta G = \Delta H_{NP-polymer} + \Delta G_{NP-NP} - T(\Delta S_{polymer} + \Delta S_{NP\text{-}position} + \Delta S_{NP\text{-}orientation}) \quad (1)$$

where $\Delta H_{NP-polymer}$ is the energetic contributions from the nanoparticle–polymer interaction, ΔG_{NP-NP} is the energy associated with nanoparticle–nanoparticle interaction, $\Delta S_{polymer}$ is the entropy associated with the polymer-chain deformation upon nanoparticle incorporation, and $\Delta S_{NP\text{-}position}$ and $\Delta S_{NP\text{-}orientation}$ are positional degree and rotational degree of freedom of nanoparticles, respectively.

With the use of a PS$_{27}$-b-PAA$_{120}$ content of 1.0 wt%, a uniform distribution of homogeneous and dense OA-MNPs on the hybrid particles was observed. With low amounts of PS$_{27}$-b-PAA$_{120}$ in the system, however, the incomplete covering of the polymer chains on the magnetic emulsion was thermodynamically unstable. As a result, the primary magnetic emulsions break, generating a random mixture with the polymer chains, which prevents an achievement of the equilibrium state. This leads to a formation of non-uniform particle clustering and aggregation of the resulting hybrid particles.[20,31] Hence, 12.0 wt% OA-MNPs and 1.0 wt% PS$_{27}$-b-PAA$_{120}$ contents were chosen for preparing hybrid MPNPs for further investigations.

3.1.3 Characterizations of hybrid MPNPs. Chemical compositions, size, zeta potential, and magnetic properties of the MPNPs fabricated by using 12.0 wt% OA-MNPs and 1.0 wt% PS$_{27}$-b-PAA$_{120}$ were examined, as summarized in Fig. 4. FTIR spectra of MPNPs and PS$_{27}$-b-PAA$_{120}$ copolymer (Fig. 4A) show characteristic bands at 2925 (C=C–H stretching), 1557, 1449, and 1404 cm^{-1} (C=C stretching), confirming the presence of PS segments. The vibrational modes at 3373 cm^{-1} (O–H stretching) and 1698 cm^{-1} (C=O stretching) of the carboxyl of PAA indicates the existence of the copolymer decorated on the magnetic clusters.[15]

Fig. 4B shows that the average hydrodynamic sizes of MPNPs compared with OA-MNPs, measured by a DLS technique, were 236 ± 26 and 164 ± 9 nm, respectively. Both the magnetic emulsion and MPNPs had a broad size distribution. From this result, the extended chain length of the hydrophilic PAA segments in the aqueous phase can be calculated by subtraction of the values, giving an average value of 36 ± 8 nm. This agrees with its negative zeta potential values at a pH range of 4–10, as illustrated in Fig. 4C. The nearly constant negative values, observed in a pH range of 6–10, are likely due to the deprotonation of the acid block copolymer to form –COO$^-$. The drastic decrease in the absolute value from −22.2 mV at pH 4 (–COOH, pK_a ~4.2) to a positive value of 15.6 mV at pH 2 originates from the protonation of –COO$^-$ of PAA.[32]

The weight compositions of the hybrid MPNPs were determined by TGA and DTG, as summarized in Fig. 5. The thermograms of MPNPs comprise three weight-loss steps at 251, 351, and 419 °C. The two lower temperature decompositions are associated with OA, a coating or stabilizing layer on the MNP's surface, as these are similarly observed in the thermograms of both OA-MNPs and MPNPs.[15] A major weight loss at 419 °C is due to the decomposition of the PS$_{27}$-b-PAA$_{120}$ matrix, where the remaining weight after this step (71.1 wt%) indicates inorganic MNPs. This value agrees with the theoretical value of expected MNP weight composition, and will be further used to verify the saturation magnetization (M_s) of the MPNPs in the VSM measurements.

Since the magnetic properties of OA-MNPs and MPNPs ensure their separation ability in practical applications, the magnetization versus applied magnetic field behavior was determined by VSM at room temperature. The results are displayed in Fig. 5B. The absence of a hysteresis loop feature in both curves confirms the superparamagnetic behavior of OA-MNPs and MPNPs. A slightly lower M_s value of MPNPs (33.2 emu g^{-1}), compared to that of OA-MNPs (39.7 emu g^{-1}), is perhaps due to the shielding effects from the PS-b-PAA matrix.[33]

The results obtained from VSM experiments can be validated by TGA results, using the following equation.:[34,35]

$$M_s = M_s^{Fe_3O_4}(1 - \chi)$$

where $M_s^{Fe_3O_4}$ is a saturation magnetization of the as-prepared Fe$_3$O$_4$ (47.4 emu g^{-1})[14] and χ is the weight fraction,
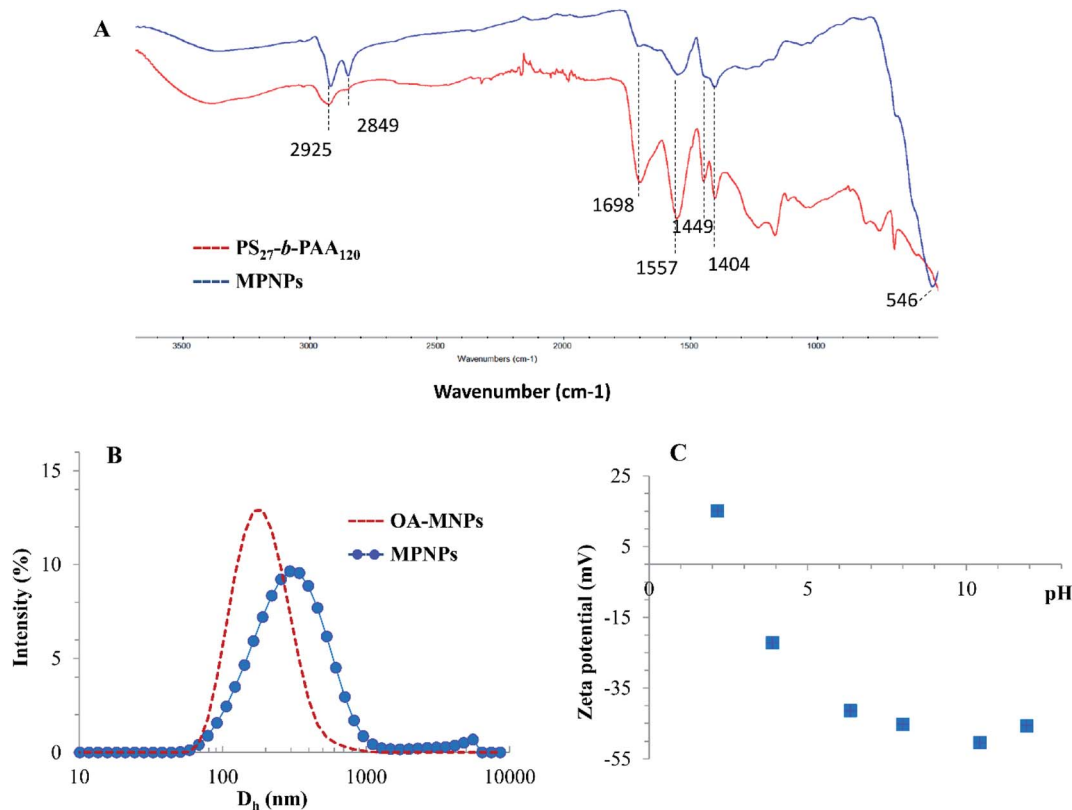
Fig. 4 (A) FTIR spectra, (B) hydrodynamic size (D_h), and (C) zeta potential of hybrid MPNPs, fabricated by using 12.0 wt% OA-MNPs and 1.0 wt% PS_{27}-b-PAA_{120}.

determined by TGA. From the equation, the calculated M_s values of OA-MNPs and MPNPs are 36.7 and 33.7 emu g^{-1}, respectively. These correlate well with those determined from the VSM measurements, demonstrating that the high-energy mixing (ultrasonication) and self-assembly processes produce the hybrid MPNPs and did not adversely affect the magnetization value.

3.2 Calcium ion removal efficiency and reusability

The adsorption efficiency of the prepared MPNPs was examined by employing Ca^{2+} as a scale-forming ion analog. The Ca^{2+} adsorption and desorption mechanisms were studied to assess the cyclability of the MPNPs by using 0.1 N citric acid as a chelating agent. The applied citric acid solution has a pH < 3. The MPNP surfaces change from negatively to positively charged, resulting in the desorption of Ca^{2+} from the particles, as proposed in Fig. 6.

The percentage removal of Ca^{2+} was 92 ± 3%, from the 1st cycle, and decreases to 55 ± 12% at the 4th cycle, as summarized in Fig. 7. The pH of the solution was set at moderately alkaline (pH 9) to conform with the typical range used in industrial cooling systems. At this pH, most of the carboxylic acid groups of PAAs were deprotonated (~92%),[36] as described above (Fig. 4C), generating –COO$^-$ groups that surround the MPNPs. The adsorption mechanism of Ca^{2+} by MPNPs is associated with the electrostatic attraction between

Ca^{2+} and –COO$^-$ on the MPNP surfaces.[7] The results from the reusability study indicate that the synthesized MPNPs can be effectively reused for up to 4 cycles, after regeneration to remove the adsorbed Ca^{2+}.

3.3 Scale-inhibition performances and mechanisms

The scale-inhibition performances of MPNPs are assessed in comparison with commercial carboxyl-based antiscalants, *i.e.*, PBTC, PMA, and Acumer 1050, as summarized in Fig. 8A. As the TGA results indicated that ~71% of the total mass of MPNPs are derived from the magnetic domains, whereas the remaining is associated with active copolymer chains, the materials were employed at an 80 ppm dosage, compared to that of 20 ppm for commercial antiscalants. The results showed that MPNPs had superior ability to inhibit the $CaCO_3$ scale, with a value of 90 ± 3%. The corresponding values for PBTC, PMA, and Acumer 1050 were 78 ± 7, 57 ± 5, and 48 ± 4%, respectively. More importantly, the prepared MPNPs can be reused, owing to their superparamagnetic property, in which a high inhibition efficiency of 70 ± 14 was still observed at the 4th cycle of application. This is likely because the long hydrophilic PAA segments can extend its chains to fully cover and stabilize the MPNPs, leading to an enhancement in exposure of their active carboxyl groups to interact with Ca^{2+} in the system.

The scale-inhibition mechanisms of the hybrid MPNPs were further investigated by observing surface morphology of the
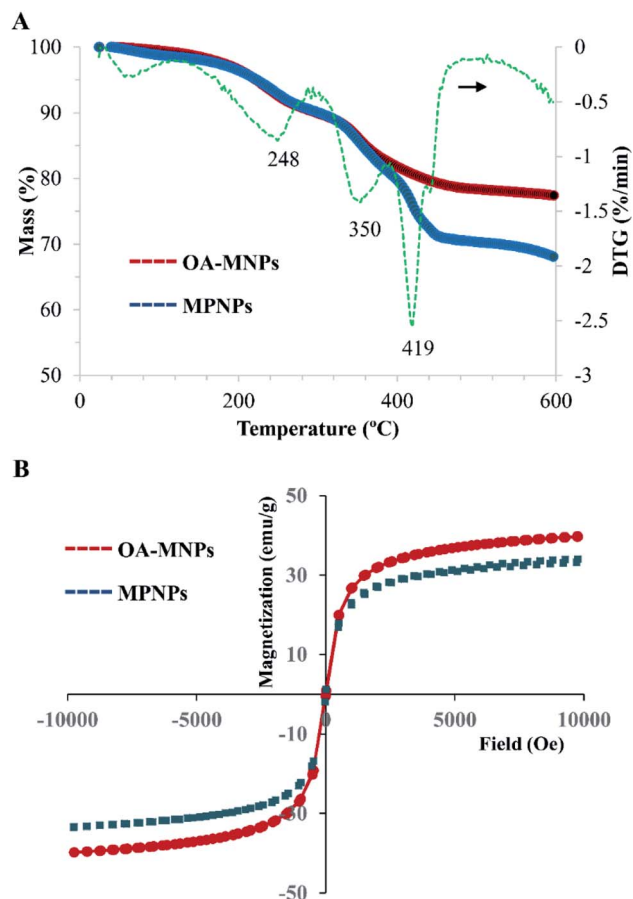
Fig. 5 (A) TGA thermograms and (B) VSM curves of hybrid MPNPs and OA-MNPs.

Fig. 7 Ca^{2+} removal percentage of MPNPs from water, as a function of treatment cycles, in a presence of MPNPs at 80 °C, pH 9, and 10 h.

precipitated CaCO$_3$ scales using SEM-EDX. The SEM micrographs of CaCO$_3$ crystals obtained from solutions without and with the application of MPNPs are compared in Fig. 8B and C. The crystals formed with an absence of MPNPs mostly showed regular shape with smooth surface, a characteristic of calcite, with some elongated crystals, which is a typical morphology of the thermodynamically-unstable aragonite polymorph (Fig. 8B).[37–39] When MPNPs were applied in the solution, a mixture of CaCO$_3$ particles
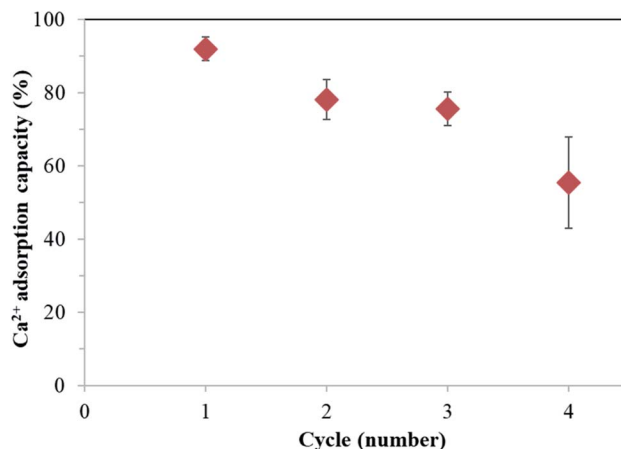
with regular shape, irregular shape (destroyed structure), and high amount of elongated crystals was observed. The calcite usually leads to harder scales, while the aragonite forms softer scales that are easier to be removed. In addition, a presence of Fe element on the CaCO$_3$ crystal's surface was detected by EDX spectra (Fig. 8E). In contrast, this could not be detected on the CaCO$_3$ scales from the blank sample (Fig. 8D). This indicates that the prepared MPNPs could not only chelate with free Ca^{2+} in the solution, but also efficiently impede the growth of CaCO$_3$ crystals by adsorbing on the forming CaCO$_3$ nanocrystals. A widely-accepted mechanism for the inhibition of CaCO$_3$ scale precipitation involves the adsorption and/or interactions of the inhibitor –COOH groups with Ca^{2+} of CaCO$_3$ crystallites. The MPNPs could capture a fraction of Ca^{2+} from the solution and thus decrease the effective supersaturation during precipitation. However, they could not stabilize the emerging CaCO$_3$ clusters or particles anymore.[5,40] The inhibition of scale formation is affected by both the location of the adsorbed inhibitor at the crystal surface and the extent of chemical bonding with the surface.[11] Therefore, the antiscalant efficiency is determined by the interactions of the scale inhibitors and the multivalent cations in the solution.
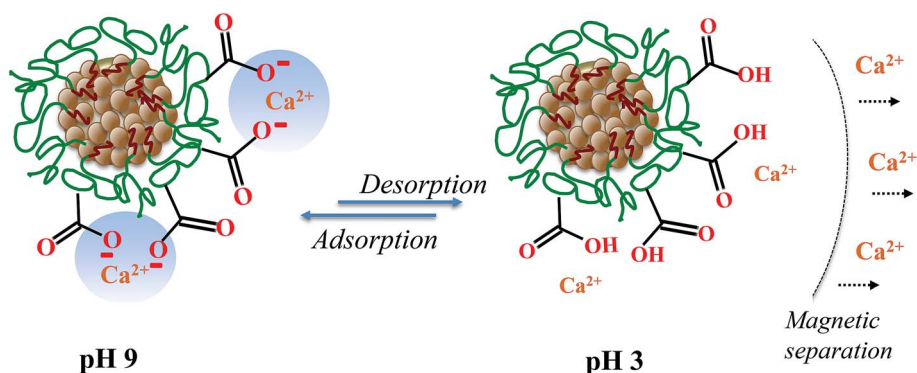

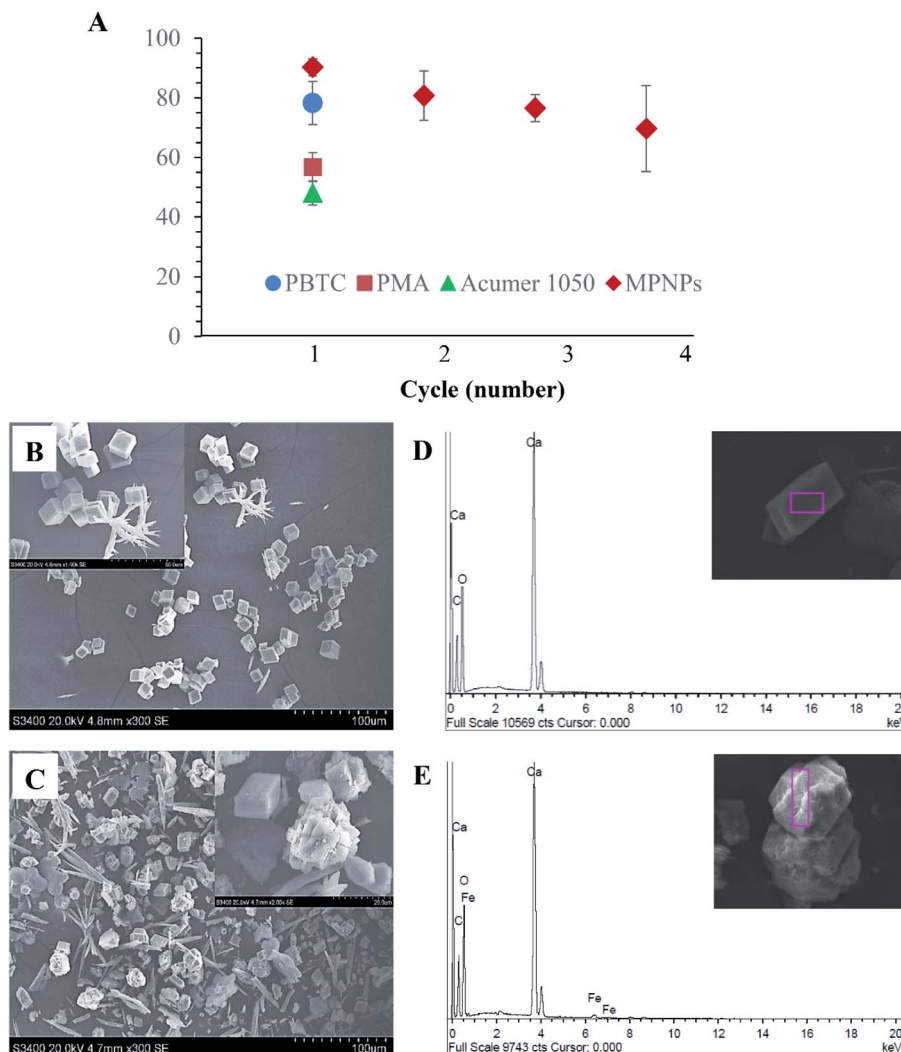Fig. 6 Proposed mechanism of adsorption and desorption of Ca^{2+} by using the prepared MPNPs.

Fig. 8 (A) Scale-inhibition efficiency of MPNPs (80 ppm) against CaCO$_3$, compared with commercial antiscalants (20 ppm), and SEM micrographs and EDX spectra of CaCO$_3$ particles formation in the solution: (B and D) in the absence of antiscalants, and (C and E) in the presence of MPNPs at 80 °C, pH 9, and 10 h.

4. Conclusions

Carboxylated magnetic polymeric nanoparticles (MPNPs) with well-defined morphology, high magnetic content (70 wt%), and superparamagnetic properties were successfully prepared. With an ultrasonication-assisted technique and a hydrophobic OA-MNP content of 12.0 wt%, a stable oil-in-water emulsion or clusters of OA-MNPs were created, without the use of organic surfactants. Although the adsorption of hydrophobic OA-MNPs in the emulsion system was thermodynamically unfavorable, self-assembly of OA-MNPs effectively stabilized the emulsions during the stabilization by amphiphilic PS$_{27}$-b-PAA$_{120}$. An addition of 1.0 wt% amphiphilic PS$_{27}$-b-PAA$_{120}$ can effectively cover and stabilize the magnetic clusters. Well-defined MPNPs without broken and reformed particles were generated. This facile methodology is highly efficient in incorporating a large number of OA-MNPs into the hybrid MPNPs. The

MPNPs (an antiscalant material in water treatment) were characterized, in terms of the degree of inhibition of CaCO$_3$ scale formation, Ca^{2+} removal efficiency, and reusability. The as-prepared MPNPs showed a Ca^{2+} removal efficiency and scale-inhibition efficiency of >90% in the 1st cycle treatment, which is superior to other commercial carboxyl-based antiscalants, i.e., PBTC, PMA, and Acumer 1050. More importantly, the particles can be reused with high efficiency for up to 4 cycles, thanks to their well-defined morphology and superparamagnetic property. In addition, these materials have high potential for use in the removal of other dangerous heavy metals in water treatment processes. They can also extract and concentrate trace amounts of metal ions in solutions, to enhance the sensitivity of detection methods.

Conflicts of interest

There are no conflicts to declare.

Acknowledgements

References

1 M. A. Tofighy and T. Mohammadi, *Desalination*, 2011, **268**, 208–213.

2 J.-S. Nam, I.-H. Baek and C. Y. Kim, *J. Am. Ceram. Soc.*, 2011, **94**, 124–129.

3 X. Guo, F. Qiu, K. Dong, X. Rong, K. He, J. Xu and D. Yang, *Appl. Clay Sci.*, 2014, **99**, 187–193.

4 Z. Amjad and P. G. Koutsoukos, *Desalination*, 2014, **335**, 55–63.

5 M. Dietzsch, M. Barz, T. Schüler, S. Klassen, M. Schreiber, M. Susewind, N. Loges, M. Lang, N. Hellmann, M. Fritz, K. Fischer, P. Theato, A. Kühnle, M. Schmidt, R. Zentel and W. Tremel, *Langmuir*, 2013, **29**, 3080–3088.

6 M. Chaussemier, E. Pourmohtasham, D. Gelus, N. Pécoul, H. Perrot, J. Lédion, H. Cheap-Charpentier and O. Horner, *Desalination*, 2015, **356**, 47–55.

7 W. Yu, Y. Wang, A. Li and H. Yang, *Water Res.*, 2018, **141**, 86–95.

8 Y. A. Maher, M. E. A. Ali, H. E. Salama and M. W. Sabaa, *Arabian J. Chem.*, 2020, **13**, 2964–2981.

9 G. Liu, M. Xue, Q. Liu, H. Yang, J. Yang and Y. Zhou, *RSC Adv.*, 2017, **7**, 24723–24729.

10 P. Xu, G. M. Zeng, D. L. Huang, C. L. Feng, S. Hu, M. H. Zhao, C. Lai, Z. Wei, C. Huang, G. X. Xie and Z. F. Liu, *Sci. Total Environ.*, 2012, **424**, 1–10.

11 B. P. H. Do, B. D. Nguyen, H. D. Nguyen and P. T. Nguyen, *Adv. Nat. Sci.: Nanosci. Nanotechnol.*, 2013, **4**, 045016.

12 C. Kaewsaneha, P. Tangboriboonrat, D. Polpanich, M. Eissa and A. Elaissari, *J. Polym. Sci., Part A: Polym. Chem.*, 2013, **51**, 4779–4785.

13 T. R. Guimarães, M. Lansalot and E. Bourgeat-Lami, *Polym. Chem.*, 2020, **11**, 648–652.

14 L. Charoenmark, D. Polpanich, R. Thiramanas and P. Tangboriboonrat, *Macromol. Res.*, 2012, **20**, 590–596.

15 C. Kaewsaneha, P. Opaprakasit, D. Polpanich, S. Smanmoo and P. Tangboriboonrat, *J. Colloid Interface Sci.*, 2012, **377**, 145–152.

16 F. Montagne, O. Mondain-Monval, C. Pichot and A. Elaissari, *J. Polym. Sci., Part A: Polym. Chem.*, 2006, **44**, 2642–2656.

17 S. Braconnot, M. M. Eissa and A. Elaissari, *Colloid Polym. Sci.*, 2013, **291**(1), 193–203.

18 R. J. Hickey, A. S. Haynes, J. M. Kikkawa and S.-J. Park, *J. Am. Chem. Soc.*, 2011, **133**, 1517–1525.

19 B.-S. Kim, J.-M. Qiu, J.-P. Wang and T. A. Taton, *Nano Lett.*, 2005, **5**, 1987–1991.

20 J. Wang, W. Li and J. Zhu, *Polymer*, 2014, **55**, 1079–1096.

21 H. Ai, C. Flask, B. Weinberg, X. Shuai, M. D. Pagel, D. Farrell, J. Duerk and J. Gao, *Adv. Mater.*, 2005, **17**, 1949–1952.

22 C. Burguière, S. Pascual, C. Bui, J.-P. Vairon and B. Charleux, *Macromolecules*, 2001, **34**, 4439–4450.

23 L. Ling, Y. Zhou, J. Huang, Q. Yao, G. Liu, P. Zhang, W. Sun and W. Wu, *Desalination*, 2012, **304**, 33–40.

24 W. J. Ahn, H. S. Jung and H. J. Choi, *RSC Adv.*, 2015, **5**, 23094–23100.

25 B. P. Binks and S. O. Lumsdon, *Langmuir*, 2000, **16**, 2539–2547.

26 H. Ma and L. L. Dai, *J. Colloid Interface Sci.*, 2009, **333**, 807–811.

27 E. Elkalla, C. Kaewsaneha and A. Elaissari, *Polym. Eng. Sci.*, 2019, **59**, E195–E199.

28 G. Qiu, Q. Wang, C. Wang, W. Lau and Y. Guo, *Ultrason. Sonochem.*, 2007, **14**, 55–61.

29 Z. Geng, Z. Cheng, Y. Zhu and W. Jiang, *J. Phys. Chem. B*, 2016, **120**, 5527–5533.

30 M. Giardiello, F. L Hatton, R. A. Slater, P. C. J. North, A. K. Peacock, T. He, T. O. McDonald, A. Owen and S. P. Rannard, *Nanoscale*, 2016, **8**, 7224–7231.

31 K. Thorkelsson, A. J. Mastroianni, P. Ercius and T. Xu, *Nano Lett.*, 2012, **12**, 498–504.

32 S. Nuasaen and P. Tangboriboonrat, *J. Colloid Interface Sci.*, 2013, **396**, 75–82.

33 L. P. Ramírez and K. Landfester, *Macromol. Chem. Phys.*, 2003, **204**, 22–31.

34 F. Lan, K.-X. Liu, W. Jiang, X.-B. Zeng, Y. Wu and Z.-W. Gu, *Nanotechnology*, 2011, **22**, 225604.

35 F. Gao, Y. Cai, J. Zhou, X. Xie, W. Ouyang, Y. Zhang, X. Wang, X. Zhang, X. Wang, L. Zhao and J. Tang, *Nano Res.*, 2010, **3**, 23–31.

36 T. Swift, L. Swanson, M. Geoghegan and S. Rimmer, *Soft Matter*, 2016, **12**, 2542–2549.

37 W. Yu, Y. Wang, A. Li and H. Yang, *Water Res.*, 2018, **141**, 86–95.

38 S. Shi, X. Zhao, Q. Wang, H. Shana and Y. Xu, *RSC Adv.*, 2016, **6**, 102406–102412.

39 L. Lin, W. Jiang, X. Xu and P. Xu, *npj Clean Water*, 2020, **3**, 25.

40 H. Wang, V. Alfredsson, J. Tropsch, R. Ettl and T. Nylander, *ACS Appl. Mater. Interfaces*, 2013, **5**, 4035–4045.